




Article

The Effect of Stochasticity of Waves on Coastal Flood and Its Variations with Sea-level Rise

Déborah Idier , Rodrigo Pedreros, Jérémy Rohmer  and Gonéri Le Cozannet 

Bureau de Recherches Géologiques et Minières (BRGM), 45060 Orléans, France; r.pedreros@brgm.fr (R.P.); j.rohmer@brgm.fr (J.R.); g.lecozannet@brgm.fr (G.L.C.)

* Correspondence: d.idier@brgm.fr; Tel.: +33-238-643-568

Received: 30 July 2020; Accepted: 2 October 2020; Published: 14 October 2020



Abstract: Coastal floods are driven by many hydro-meteorological forcing factors, among which are mean sea levels, tides, atmospheric storm surges, and waves. Depending on these conditions, wave overtopping may occur and, in some cases, lead to a significant flood. In the present study, we investigate the effect of the stochastic character of waves on the flood itself using a phase-resolving wave model (SWASH). We focus on the macro-tidal site of Gâvres (France), consider two past flood events (both resulting from wave overtopping), and investigate how the effect of randomness of waves on the flood is changing with the forcing conditions and the time span (minutes to hours). We clearly show that the effect of waves' stochasticity on the flood itself is far from being negligible and, especially on a short time scale (~15 min), generates an uncertainty comparable to that induced by the sea-level rise scenarios, as long as the still water level remains smaller than the critical level above which overflow occurs. This implies that lower confidence should be assigned to flood projection on sites where wave overtopping is the main process leading to flood.

Keywords: hydrodynamic modeling; SWASH; seed; Gâvres; overtopping; sea-level rise; uncertainties

1. Introduction

Coastal floods are driven by many hydro-meteorological forcing conditions, among which are mean sea levels, tides, atmospheric storm surges, and waves. Coastal flood modeling made significant progress these last years, especially in the estimation of floods induced by wave overtopping [1,2]. A widely used approach is to first propagate the water levels and waves close to the coast using most of the time shallow-water and wave spectrum models, respectively, and then to model the flood, i.e., the water height and current inland, and deduce flood information (e.g., water height map, hazard map, flooded area, seawater volume). In case the flood is mainly induced by overflowing of the coastal defenses, shallow-water models are able to properly reproduce the hydrodynamics [3]. In the case of wave overtopping, a widely used approach is to apply wave overtopping formulas (see e.g., [4]) to estimate discharges as inputs of shallow-water models [5]. These formulas require the estimation of the wave height and period at the toe of the structure and provide estimates of the mean discharge and, for instance, the 90% confidence interval. However, these formulae have some limits, among which is the fact they are designed for specific hard defenses and thus are not adapted to the natural environment or unclassical coastal defenses [4]. In these cases, a solution is to use, for instance, phase-resolving wave models [6,7]. These models require instantaneous high frequency (e.g., >1 Hz) water level time series as forcing conditions, including the mean sea level, tide, atmospheric surge, but also the waves. Indeed, in the real world, this is a single water level time series (including all these components) that occurs in any location. To account for the wave contribution, a time series has to be extracted from the modeled wave spectrum. However, an infinite number of time series could occur for a same-wave spectrum [8], which is the cause of stochasticity or randomness of waves investigated in this paper.

Using a shallow-water and Boussinesq model, Ref. [9] tested the sensitivity of overtopping to different random phase distributions for the amplitude components of a wave spectrum and found a ratio of minimum to maximum volume of about 2, for time span containing 250 waves. As reminded in [10,11] raised the issue of the relationship between the length of the time series and the accuracy of the wave overtopping estimate. Ref. [12] recommends simulating a sequence of 1000 waves for each sea state tested. Refs. [11,13] noticed that the overtopping discharge from tests using series of 500 waves is very close to that from tests with 1000 waves, while Ref. [14] shows that using more than 1000 waves does not affect the overtopping estimate (mean and level confidence). Indeed, the effect of the stochastic character of waves on overtopping discharge (and thus floods when they are driven by overtopping) depends also on the time span during which the parameters influencing the waves are almost constant. For instance, considering a wave period of 12 s, a time span of 1 h 40 min would allow 500 waves to reach the coast. However, along macro-tidal coasts, in particular, nearshore waves are modulated by tides (see e.g., [15]) such that water level can exhibit changes up to a few meters in a single hour. Thus, we could expect a significant effect of the stochastic character of waves on floods. A way to investigate (and account for) this effect would be to replicate experiments for the same forcing conditions (e.g., still water level and wave spectrum) but for different wave time series generated from the wave spectrum. However, for real sites subject to overtopping, the few coastal flood modeling done using phase-resolving models (see, e.g., [1,7]) usually account for single time series such that, to our best knowledge, this problem of the effect of the stochastic character of wave on flood itself has rarely been tackled in the literature.

The present work aims at investigating the influence of the stochastic character of waves on coastal floods for different flood regimes. This work is done on the real site of Gâvres (France), which is subject to flood induced by overtopping and has faced several floods since 1900 [2]. We show that the stochasticity of waves is far from being negligible, especially for floods resulting mainly from wave overtopping, and, depending on the flood regime, this effect is comparable to that of sea-level rise scenarios of few tens centimeters, for the past reference events we consider in this work. First, the site, the flood model, and the method are described (Section 2). Results are provided in Section 3. The method, results, limits, and implications are discussed (Section 4) before drawing the conclusion.

2. Materials and Methods

2.1. Site Description

Gâvres is located on the French Atlantic coast (Figure 1a) in a macro-tidal environment (mean spring tidal range: 4.2 m). Its surface is smaller than 2 km². The last major flood occurred on 10 March, 2008 (Johanna storm). During this event, about 120 houses have been flooded (Figure 2, purple dots). This flood was mainly related to overtopping processes [1,16]. After Ref. [2], this site has been subject to 9 flood events (including 5 major floods) between 1900 and 2010. The waves arriving at the coast are affected by the presence of an offshore island (Groix) located at the West of the study site (Figure 1a), such that the offshore wave conditions between the site and Groix are strongly non-uniform. After some wave modeling tests (not shown), the local non-uniform wave conditions are found to result mainly from the propagation of wave conditions observed South of Groix (Figure 1a, green star).

The coast of Gâvres exhibits a wide variety of waterfront (Figure 3, satellite image and photos): the south-west end is made of soft cliffs, the tombolo (at the East, outside the study area) is made of sandy dune, while most of the rest of the shoreline is characterized by hard coastal defenses of different types. The main part of Grande Plage (P2, P3) is protected by 3 to 4 m high sea walls with a riprap recovered by a concrete layer and a promenade on the top, with an additional low stone wall inland. On the photos (P2, P3, captured in 2017), most of the coastal defenses are recovered by sand (there has been massive sand nourishment in 2012). At the south end, a stone sea wall is found, with some riprap (P4). Along the opposite coast, at P5, a sea wall with riprap recovered by a concrete layer is also found. At the North, and until the tombolo, only seawalls are found (P6, P7). Figure 3

shows the corresponding topo-bathymetric profile, representative of the 2008 configuration. At that time, especially in Grande Plage, the beach level was much lower. After the 2008 flood event, coastal defenses have been slightly raised by overlapping a layer of parapet concrete blocks in some locations, and by massive sand nourishment, as well as a groyne construction at the East of our study area (for an overview of the historical evolution from the first coastal defenses in 1830 to 2005, see [17]). In the present study, as a topo-bathymetric configuration, we consider the one contemporary of the Johanna flood event, i.e., the one of 2008.

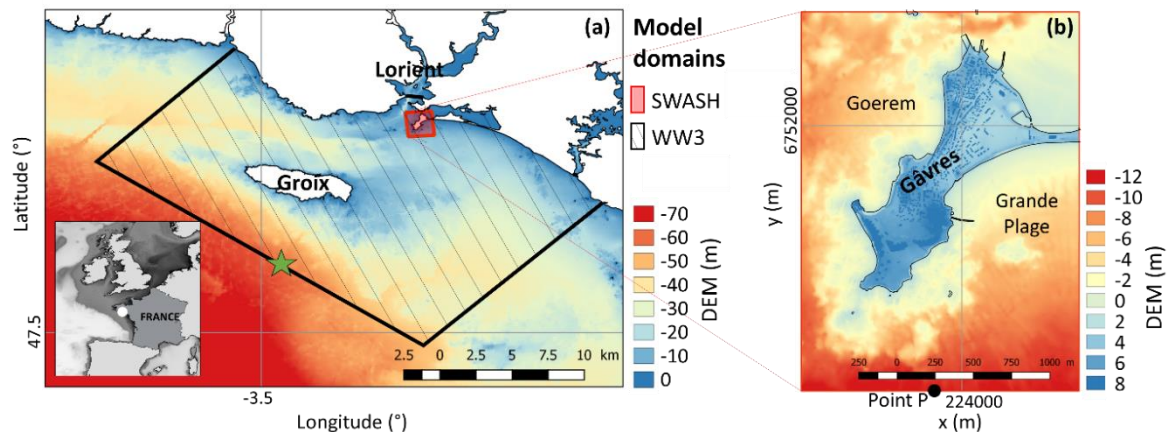


Figure 1. Location and topo-bathymetry of the study site (a,b) and computational domains of the models (WW3 and SWASH) of the modeling chain (a). The green star indicates the location of the offshore wave forcing. The topo-bathymetry is shown in terms of elevation with respect to the national vertical reference datum (IGN69). Adapted from [2].

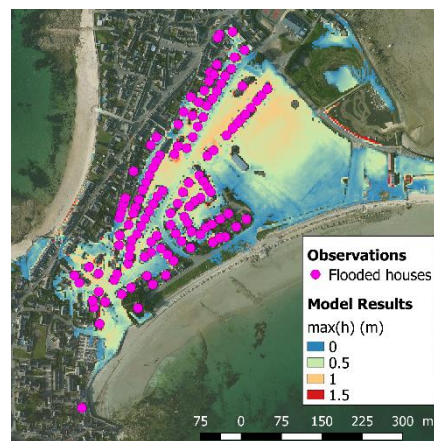


Figure 2. Model validation: maximal simulated water depth and observed flooded houses for the Johanna event. Adapted from [2].

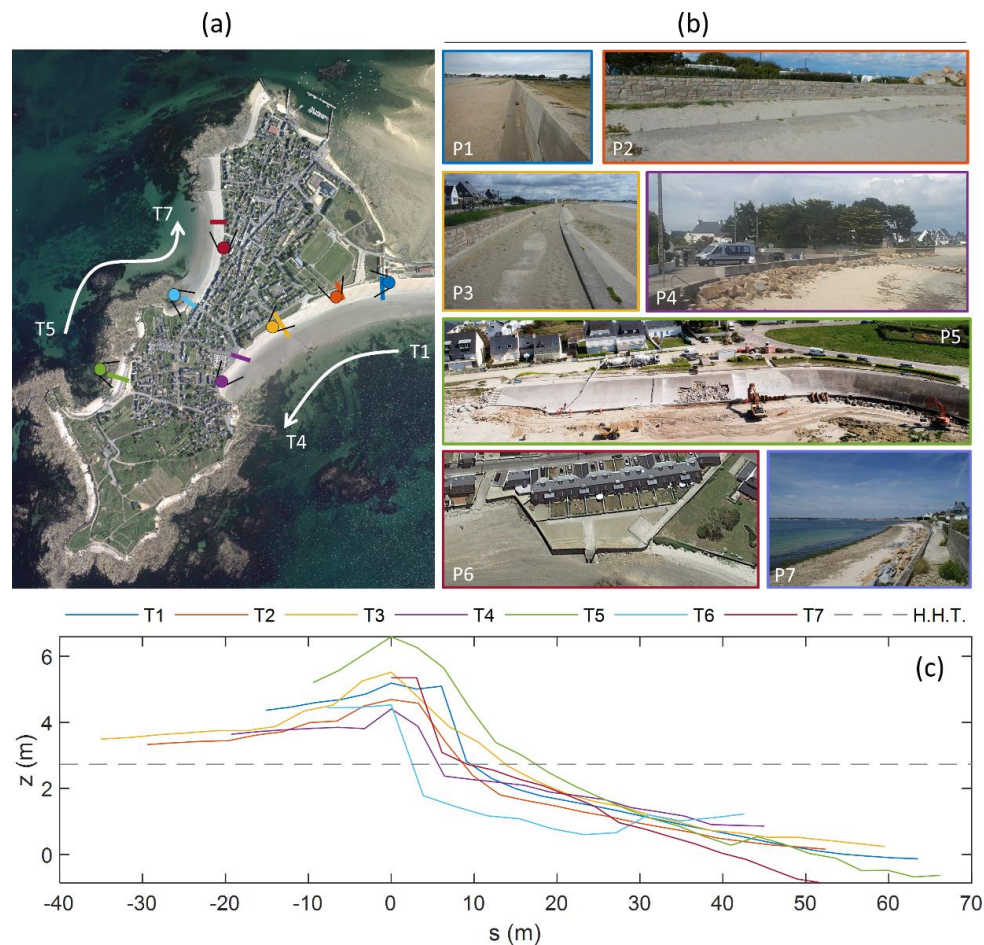


Figure 3. Aerial photo of Gâvres (a), local photos (b), and topo-bathymetric transects (c). (a): the colored circles and associated black lines indicate the location and direction of the shootings P1 to P7, the colored lines indicate the location of the transects T1 to T7, the colors of the circles and lines refer to the frame color of the local photos (b) and to the line color (c). (c): topo-bathymetric transects extracted from the digital elevation model “DEM2008” (see Section 2.2) with a vertical reference corresponding to the national datum IGN69. To be noted: the photos (b) are not contemporary of the DEM2008 (the oldest, P1, has been acquired in 2011, the other ones have been acquired in 2017 or latest). Sources of photos: IGN (a), BRGM (b, P1 to P4), © FlyUp Drone (b, P5), Google Earth (b, P6), André C. (b, P7).

2.2. Model Setup and Validation

In the present study, we use the non-hydrostatic phase-resolving model SWASH [6,18] to model the flood as it allows simulating wave overtopping and overflow. Due to computational constraints, when the phase-resolving mode of SWASH is used, this model cannot be applied to very large domain. Thus, the computation domain is restricted to the Gâvres site (Figure 1b) and we first downscale the wave conditions offshore Groix (significant wave height H_s , peak period T_p , peak direction D_p) to the boundaries of the SWASH model (Figure 1b) using the spectral wave model WW3 [19], assuming that the wave spectrum follows a Jonswap spectrum with a directional spreading of 30° , and taking into account the local wind (wind intensity U , wind direction D_u) and still water level (SWL; including: mean sea level, tide, and atmospheric surge). The WW3 computation domain is shown in Figure 1a (in black). SWASH is run with the non-uniform wave boundary conditions and spatially uniform still water level (spatially uniform sea-level, tide, atmospheric surge) and local wind. We should remind that the SWASH code, solving also the non-linear shallow-water equation, accounts also for the wave set up near the coast and that the forcing boundaries of SWASH (south and west boundaries) have been taken deep and far enough from the coast to ensure they are outside the surf zone. The space and

time resolution of SWASH is, respectively, 3 m and more than 10 Hz. On the vertical, a discretization of two layers is used. The topography and bathymetry are built based on bathymetric surveys (done by SHOM and DHI), lidar (public RGE ALTI IGN product), and GPS field survey. The resulting digital elevation model (DEM2008) is representative of the 2008 topo-bathymetry (Figure 1b). The spatial changes in the bottom roughness (related to land use) are taken into account, following the same approach as in [1]. In its present state, in 2D or quasi-3D configurations, the SWASH code cannot deal, at the same time, with low frequency (e.g., tide) and high frequency (e.g., waves) changes in the water level. To overcome this issue, in case of low-frequency changes in forcing water levels (e.g., tides), the simulation period is divided into Nt time steps of 10 min, such that there is one SWASH simulation over 10 min for each of these time steps, with hot starts from the previous run.

This model chain has been validated in terms of flooded area on the 10/03/2008 event [2]. The forcing conditions used to model this event are shown in Figure 4 (in blue). The still water level was extracted from modeling [1] done with a shallow-water model (MARS, [20]) accounting for both tide and atmospheric storm surges. In this dataset, the atmospheric storm surge exceeds 0.7 m during the rising tide and reaches about 0.55 m at high tide. The wave conditions come from the Norgasug hindcast [21]. This wave hindcast has been done with the WW3 spectral wave model [19]. The wind has been extracted from the Climate Forecast System Reanalysis [22], done with a global, high-resolution, coupled atmosphere-ocean-land surface-sea ice system, with data assimilation. Our modeling chain has been run on 6 h, centered on the high tide, using these unsteady forcing conditions. An animation of the simulated 2008 flood event is provided in the supplementary material. It illustrates how the water level spatio-temporal changes, the wave overtopping, and inland flood are reproduced with the model. The modeled flood extension exhibits a good agreement with the observations, i.e., the locations of houses known to have been flooded during the Johanna storm (Figure 2).

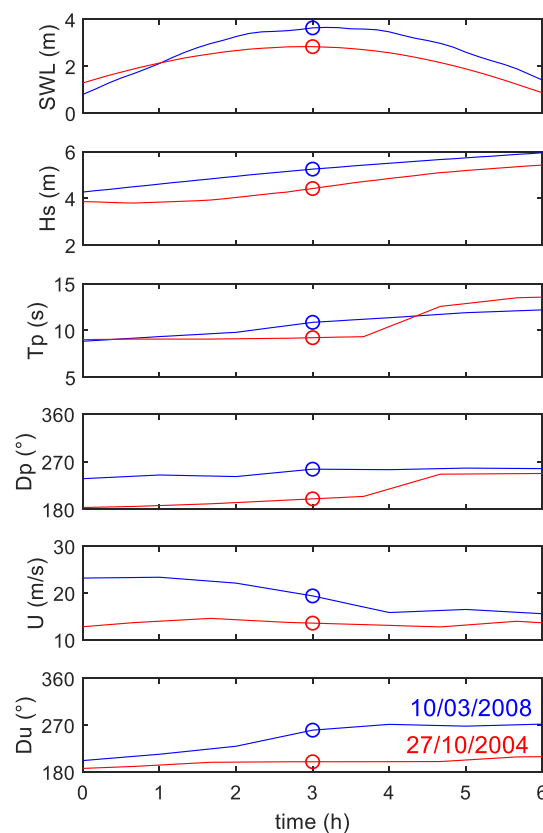


Figure 4. Forcing conditions of the modeling chain, for the 27/10/2004 (in red) and 10/03/2008 (in blue) events, from high-tide minus 3 h to high tide plus 3 h. The still water level (SWL) is given with respect to the national vertical datum IGN69.

In the present work, we will mainly use the water height computed in each inland cell of the computational domain (Figure 1b) to deduce several types of information (see Section 2.3).

2.3. Modeling Experiment

For a given still water level, in the SWASH model, the generation of instantaneous (i.e., high frequency) water level time series from a single wave spectrum is based on the modification of the phases of the components in the Fourier space, thanks to the user parameter named *seed*. Replicating simulations with different *seed* values allows generating different time series. In our study, in each simulation, we randomly selected the *seed* number. In the simulation presented in Section 2.2 (2008 flood event), we used the default value of the *seed* parameter.

In the present work, we focus on two hydro-meteorological events that occurred at Gâvres (Figure 4): the 27/10/2004 event, which induced only limited wave overtopping (local observations, see [2]), and the 10/03/2008 event, which led to a significant flood. In terms of variable of interest, we mainly consider the probability (p) of each grid cell to be flooded and the volume (Vol) of water entering inland during the period of interest. Contrary to most of the studies focusing on wave overtopping volume computation, the volume computed here is not computed along a cross-shore transect but, instead, is obtained by summing the water volume (height \times grid cell surface) of each inland cell of the computational domain (Figure 1b), as an indicator of the flood on the hinterland of Gâvres. Three types of events are considered:

- a first type on 6 h with unsteady forcing conditions (called E6hUS),
- a second type on 20 min with steady forcing conditions (called E20mS),
- a third type on 6 h but with steady forcing conditions (called E6hS).

The first type of simulations (E6hUS) allows investigating the two past real events of 27/10/2004 and 10/03/2008. However, as the computational time is significant (60 h per simulation on 48 cores), only a limited number of repetitions of the simulations can be done, such that we repeat these simulations only 5 times for each of the two events. For such type of 3D wave simulations with time-varying still water level, 10 min sub-simulations are done with hot-start (see Section 2.2). However, the wave generator (in the SWASH model) does not see the generated wave time series of the previous sub-simulation, such that it starts from scratch. Thus, to limit (10 min) cyclic effect, the seed value is randomly selected at the beginning of each 10 min sub-simulation. The second type of simulation (E20mS) is less computationally expensive (3 h on 48 cores) and focuses on high tide hydro-meteorological conditions for each of the 2004 and 2008 events (circles in Figure 4). We use this type of simulation to: (1) repeat simulations a large number of times (here 66 times, which allows estimating up to the 95th percentile at 95% confidence level following Wilks formula [23]), (2) make additional scenarios around the 2004 and 2008 ones, by accounting for larger still water levels ($\Delta SWL = 0.05, 0.1, 0.2, 0.5, 1, \text{ and } 1.5 \text{ m}$). These scenarios of SWL increase can be seen as scenarios accounting for changes in the tide and surge components but also for sea-level rise. Indeed, according to the latest Intergovernmental Panel on Climate Change report [24], sea level is projected to rise by 0.61–1.10 m by 2100 (likely range) under RCP8.5 (high greenhouse gas emissions) and to continue rising for centuries. The projected likely range could be exceeded, for example, with large melting of Antarctica's ice sheets involving marine ice cliffs instabilities [25]. The literature available today commonly gives sea-level scenarios by 2100 in the order of 1.5 m or more under these unfavorable settings [26–28]. With these tests, we aim at comparing the effect of wave stochasticity to the effect of increases in the components of SWL (i.e., mean sea level, tide, or atmospheric surge). Finally, the last type of scenarios (E6hS), for which we can afford only a limited number of simulations due to too high computational cost (here: 5), is used to better investigate how the effect of the stochastic character of waves is changing with the time span.

For 2004 (2008) events, at high tide, the wave peak period is equal to 9.2 s (10.9 s). This implies that to get series of, for instance, 500 nearshore waves, a time span of 1.3 h (1.5 h) would be necessary. In such a time span, we can observe still water level changes of ~10 cm (around the high tide) to ~1 m

(around mid-tide) over the tide cycle of the two events. This suggests that we may observe the effect on the stochastic character of waves on the flood on this study site.

2.4. Preliminary Estimation of Inland Water Volumes Induced by Overflow

Before investigating the stochastic effect of overtopping waves on the flood, a preliminary analysis of the inland water volume induced by overflow is made under strong simplifications. We assume that the inland water volume is a function of the still water level (i.e., the water level resulting from the mean sea level, tide, and atmospheric storm surge), and apply a bathtub method accounting for the connectivity (see, e.g., [29]) to the DEM2008 digital elevation model (described in Section 2.2). The bathtub flood model assumes that each DEM cell with an elevation less than the still water level and hydrologically connected to the sea (i.e., the model account for the passage of water from one cell to another) is flooded. The water height in each flooded cell is equal to the still water level minus the ground level. By summing the obtained water height in each inland cell and multiplying it by the grid cell size (9 m^2), we obtain the inland water volume. As reminded by [30], the bathtub technique can lead to overestimation due to simplifications of physical processes (it neglects terrain roughness, timing/duration of the event, and flow velocity that affects the landward propagation distance from the coast). In the present study, we use this method only as a preliminary analysis to provide a major value of water volumes inland resulting from overflow processes in the absence of waves and to identify still water level thresholds. Figure 5 (black line) shows the increase of the volume with the still water level, but also the threshold ($\text{SWL}_C = 3.77 \text{ m}$ in the official French vertical datum IGN69), above which overflow occurs. It also shows (filled circles) that the 2004 event SWL is far from inducing flooding by overflow and that the 2008 event SWL is close to the critical conditions, but is still smaller.

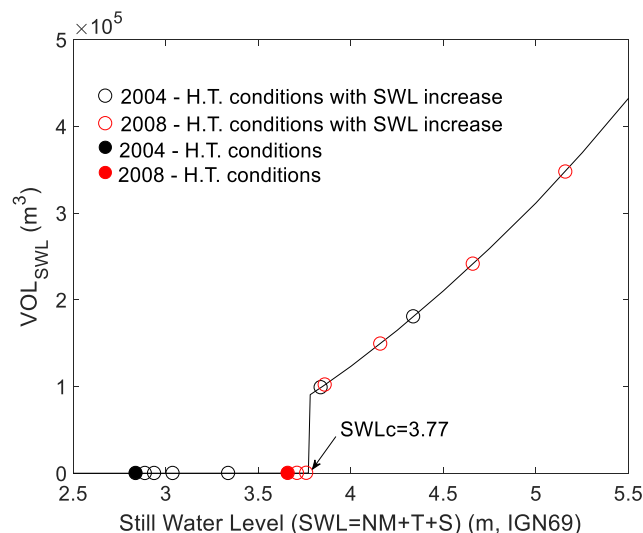


Figure 5. Inland water volume obtained using the bathtub method (with connection to the sea). The filled black and red circles indicate the high-tide conditions (still water level) of the 2004 and 2008 events. The black and red empty circles indicate the volume obtained for larger still water levels, corresponding, for instance, to climate change-induced sea-level rise scenarios of [0.05 0.1 0.2 0.5 1 1.5] m. The arrow indicates the still water level threshold (SWL_C) above which overflow occurs.

Taking into account the wave setup contribution, the water level slightly increases but remains smaller than SWL_C . Indeed, as a very crude approximation, numerical simulations (with the model described above) of the 2004 and 2008 events (i.e., for the conditions corresponding to the circles in Figure 4) show that the maximal wave setup along the coast of our study site is about 10 cm at high tide.

Figure 5 and the above discussion on wave setup contribution confirms that these past flood events have been triggered by wave overtopping processes. In addition, after these estimations, increasing the high tide level of the 2004 (2008) event of 1 m (0.2 m) would lead to overflow.

3. Results

3.1. Wave Stochasticity Effect on the 2004 and 2008 Flood Events (Unsteady Forcing Conditions)

Figure 6 shows the high-frequency (1 Hz) water level time series at the southern boundary of the SWASH computational domain (point P in Figure 1b), for the 2004 and 2008 events, and for the 5 simulations of each event (E6hUS simulations). These time series include the mean sea level, tide, atmospheric surge, and the waves and illustrate the stochastic character of the waves: the same offshore wave forcing leads to different surface elevation time series. The question is: does this stochastic characteristic influence the flood on our study site, and to which extent? First, the model results (Figure 7) show that the maximal inland water height in each grid cell is not constant through the 5 simulations, suggesting that the stochastic character of waves has an impact on the flood on our study site. To better quantify this effect, the flood probability (p , computed in each grid cell, using the 5 simulations done for each event) is analyzed. If there were no significant effect of the wave stochasticity on p , there should be a single mode, equal to 1, because all 5 runs would flood exactly the same grid cells. Figure 8a,b shows that this is not the case. While the 2008 event provides the main mode at 1 but still values to 0.2, the 2004 event leads to much more heterogeneous probabilities, with the main mode at 0.2. This means that most of the flooded cells are flooded only in 1 simulation over the 5 simulations, or, in other words, that the flooded cells differ from one simulation to another. The analysis of the maximal water volume inland (Figure 8c) also highlights the effect of the stochastic character of waves, for the 2008 event and (even more) the 2004 event, where the maximal volume exceeds 1.1 and 10 times the median, respectively. Focusing on flood events induced by wave overtopping, this illustrates that, not only small flood events but also large flood events (even if to a smaller extent) are sensitive to the effect of wave stochasticity.

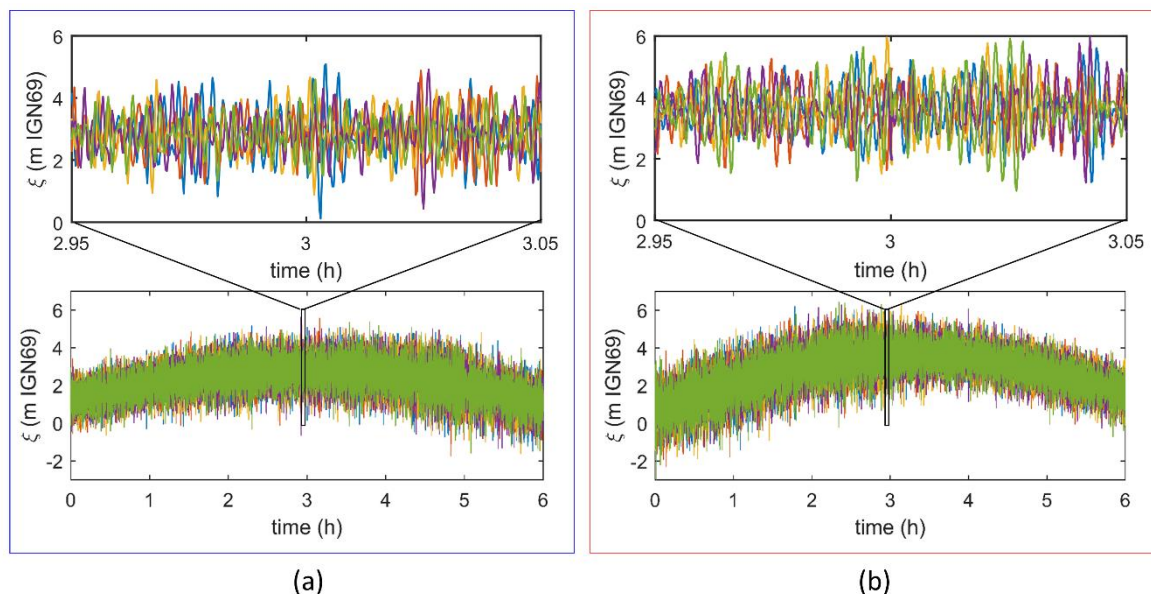


Figure 6. Instantaneous water level (denoted ξ) at the southern boundary (point P, Figure 1) of the computational domain of the SWASH model, for the 27/10/2004 (a) and 10/03/2008 (b) events, with 5 simulations per event.

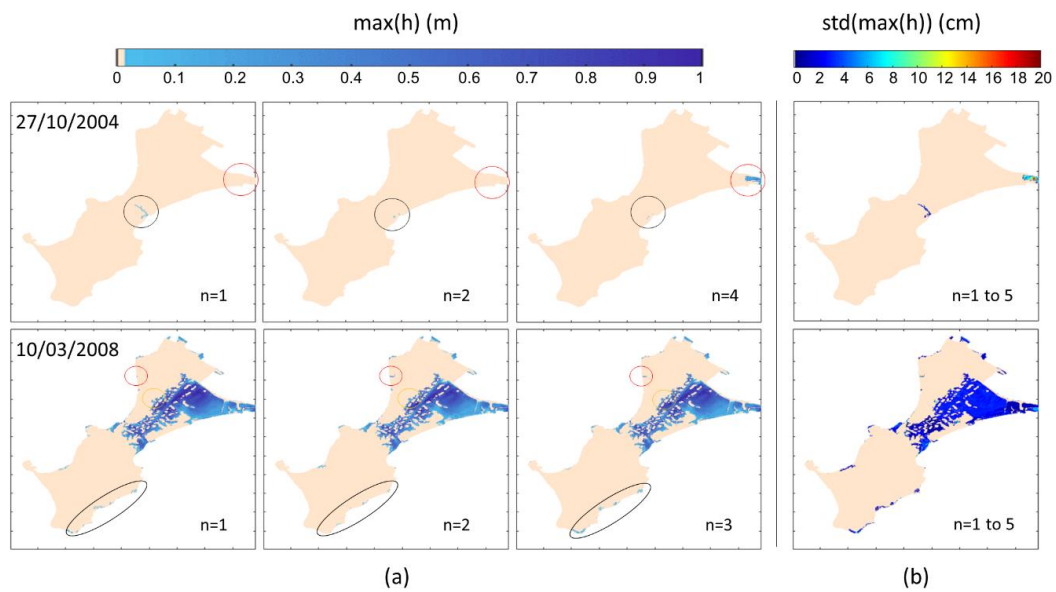


Figure 7. Flood results for the 24/10/2004 (top panel) and 10/03/2008 (bottom panel) events: (a) maximal inland water height for a subset (for sake of figure readability) of the 5 simulations done for each event, (b) standard deviation of the maximal inland water height, computed using the results of the 5 simulations. For each of the two events, the circles highlight some of the areas of differences between the results.

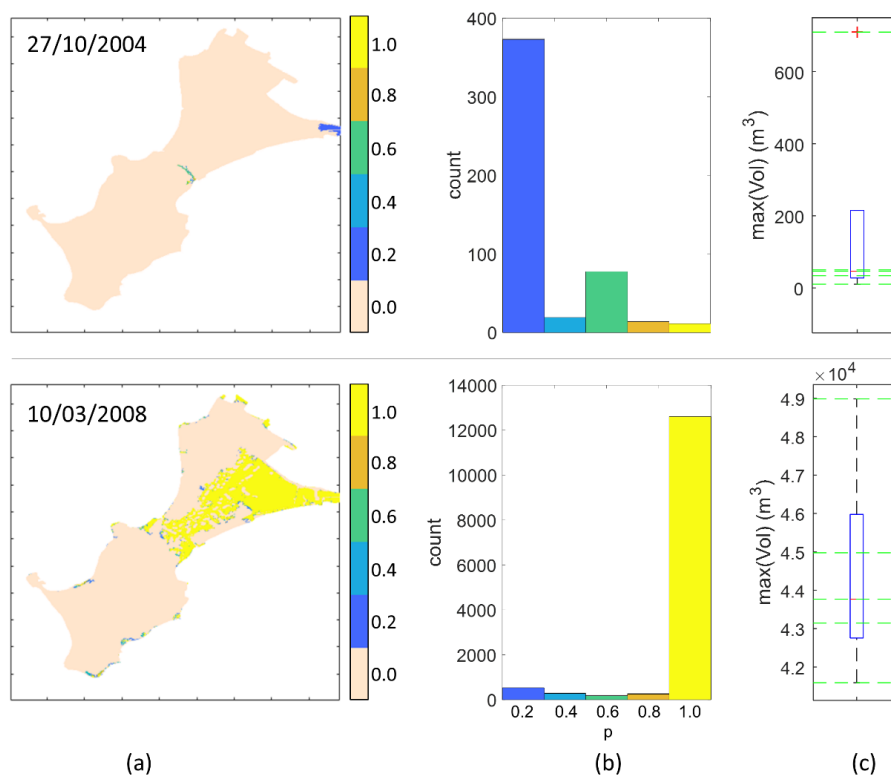


Figure 8. Flood results for the 24/10/2004 (top panel) and 10/03/2008 (bottom panel) events, computed using the 5 simulations done for each event: (a) flood probability $p(x,y)$, (b) flood probability histogram for $p > 0$ (c) boxplot of the maximum of water volume inland, with the green lines indicating the computed value for each of the 5 simulations. On each boxplot, the central red mark indicates the median, and the bottom and top edges indicate the 25th and 75th percentiles, respectively. The whiskers extend to the most extreme data points not considered outliers. The outliers are plotted individually using the '+' symbol.

3.2. Wave Stochasticity Effect on Flood at Few Minutes Time Scale and for Still Water Level Increase Scenarios (Steady Forcing Conditions)

Considering the E20mS simulations (Section 2.3), Figure 9 shows boxplots of maximum inland water volume (considering 66 simulations for each event) versus the still water level. The results obtained for $\Delta\text{SWL} = 0$ correspond to the forcing conditions that occurred at high tide for each of the two events (2004 and 2008). First, as in the case of unsteady forcing conditions, the inland water volume depends on the simulation considered in the 66 simulations, illustrating that the stochasticity of waves has an effect on the flood on the considered short time span of 20 min. It should be noticed that these 20 min simulations include the spin-up. For both events, the spin-up is about 5 min.

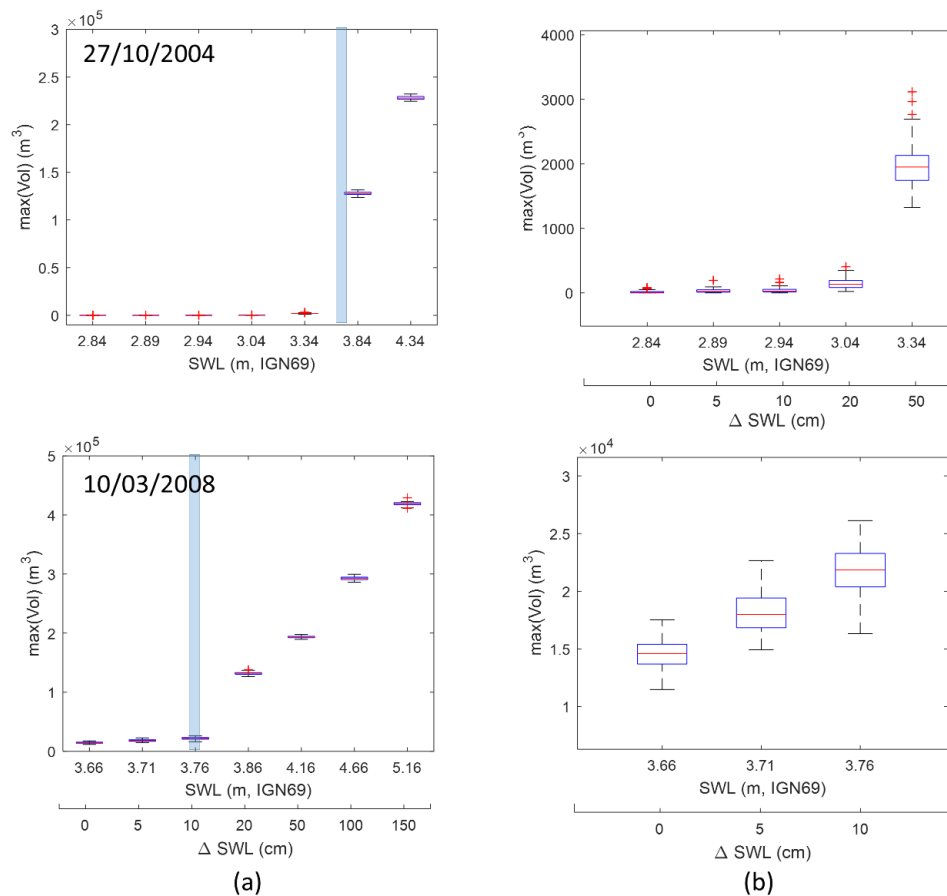


Figure 9. Boxplot of maximum inland water volume (considering 66 simulations for each event) versus the water level (and the still water level increase compared to the reference events) for the 2004 (top panel) and 2008 (bottom panel) events. (a) full results (with the blue vertical bar indicating the critical still water level SWL_C for overflowing without waves, see Section 2.4), (b) zoom on the left part of (a), for $\text{SWL} < \text{SWL}_C$. To be noted: the SWL and ΔSWL axis have different units (m and cm, respectively).

As expected, the water volume is increasing with SWL increase (Figure 9a). It is increasingly akin to the volume computed with the bathtub method (Figure 5), even if values differ: (i) for $\text{SWL} < \text{SWL}_C$, the water volume is very small and slightly increases with SWL, (ii) for SWL close to SWL_C , there is a sudden jump, (iii) then for $\text{SWL} > \text{SWL}_C$ (i.e., a still water level larger than the critical water level above which overflow dominates), the volume is increasing much faster.

Figure 9 shows also that for $\text{SWL} < \text{SWL}_C$, the effect of the stochastic character of waves on the inland water volume is larger than the one of still water level increase, i.e., starting from $\Delta\text{SWL} = 0$, the whisker width of each boxplot is larger than the effect of incremental increase in still water level (looking, for instance, at the difference between median values for successive boxplots). To provide

some magnitude order in the case of a significant flood, let us consider the 2008 results for $\Delta\text{SWL} = 10$ cm (10 cm is typically a sea-level rise value that could be reached in a few decades): the stochastic character of waves induces variations of $10,000 \text{ m}^3$ to be compared to the median value of about $22,000 \text{ m}^3$, i.e., about 50% of the median value. For $\text{SWL} > \text{SWL}_C$, even if not negligible, the effect of the wave stochasticity on the inland water volume becomes smaller than the effect of incremental increase in still water level. Again, let us consider the 2008 results, but for $\Delta\text{SWL} = 50$ cm (i.e., $\text{SWL} > \text{SWL}_C$): the stochastic character of waves induces variations of 8234 m^3 to be compared to the median value of about $193,374 \text{ m}^3$, i.e., about 4% of the median value.

As a conclusion, on the considered time scale (~ 15 min), the stochastic character of waves has an effect on the flood larger than the effect of the still water level increase, as long as the still water level is smaller than the critical one above which overflow occurs. This still water level increase can be due either to higher high tide (or storm surge) than the one of the considered events or to the climate change-induced sea-level rise.

3.3. Wave Stochasticity Effect on Flood at Few Hours Time Scale (Steady Forcing Conditions)

Additional simulations have been done considering the high tide forcing conditions of the 2004 and 2008 events (without any still water level change anymore) and a longer time span (6 h to compare to the 20 min). This corresponds to the E6hS type of event (Section 2.3). The comparison of the results obtained for both time spans (Figure 10) shows that the longer the time span (i.e., the duration of the simulation), the more likely it is that all 5 simulations predict exactly the same flooded pixels and, therefore, the more likely it is that the probability p is equal to 1 on the flooded pixels. However, even on a 6 h time span of steady forcing conditions (a case which would never happen on the field), there are still cells with p values smaller than 1. For the 2004 event, the p values are well spread between 0.2 and 1, meaning that even if some cells are flooded in each simulation ($p = 1$), most of the flooded cells are flooded only for a subset (4 to 1) of the 5 simulations. This means that the stochastic character of waves has still an effect on the flood. As expected, this effect after 6 h is larger for the 2004 case where only a few waves overtop, to compare to the 2008 case, keeping in mind that the 2004 forcing conditions let to a much smaller flood extent (1% of the 2008 case).

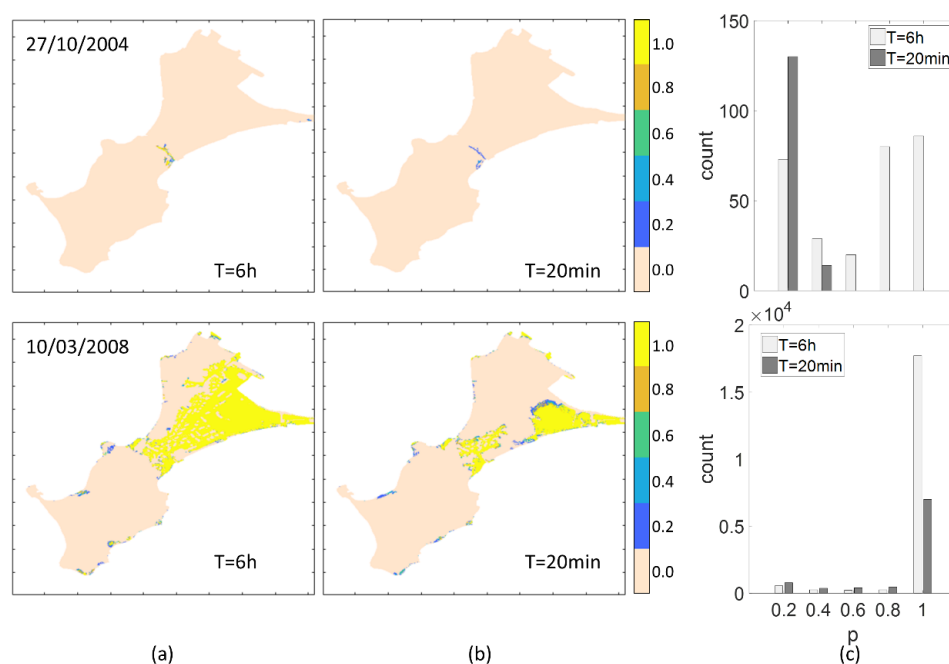


Figure 10. Flood probability map for the (a) E6hS and (b) E20mS runs. (c) Resulting flood probability (denoted p) histogram (count corresponds to the number of cells). Probabilities p are computed based on 5 simulations for each event.

4. Discussion and Conclusions

To the authors' best knowledge, this is the first time that the effect of the stochastic character of waves on the flood itself, on a real site and in 2D dimension (i.e., not longshore uniform coast), has been investigated and quantified.

In the present study, we focused on one site and two reference (past) events (around which we investigated the SWL effect). The simulation of both events (with unsteady forcing conditions, i.e., accounting for time-varying tide, storm surge, waves, and wind) provides flood extent in agreement with the local observations and illustrates not only the significant effect of tide on the flood but also the stochastic effect of waves on the flood, with an effect much larger for the 2004 than for the 2008 event. This effect depends on the number of overtopping waves. For instance, the analysis of the stored water height maps (1 min time step) shows that at least 1 to 2 (several tens) waves overtopped the coastal defenses for the 2004 (2008) event, consistently with the found larger wave stochasticity effect on flood for the 2004 event, and with the resulting flood, which is much smaller for the 2004 event. Investigating more systematically how the wave stochasticity effect on the flood is changing with the flood intensity would allow to better identify if and under which conditions there may be significant uncertainties in deterministic flood predictions.

Our additional simulations, done for steady conditions over 20 min but also 6 h time spans, suggest that the stochastic character of waves could also play a significant role in micro-tidal areas. This could be argued that 20 min is short compared to typical storm durations (hours to days), but the 6 h simulation results (especially for the 2004 event high tide conditions, where the number of overtopping wave is limited) show that there is still an effect of the stochastic character of waves on the flood. Thus, this effect may be encountered also in micro-tidal area and could be significant when the surge, during a short time span, is large enough to allow the overtopping of a limited number of waves. This deserves to be further investigated/confirmed by flood modeling experiments accounting for real unsteady forcing conditions in micro-tidal sites subject to wave overtopping.

The two investigated events are characterized by very different forcing conditions (Figure 4), leading to a larger flood for the 2008 event than for the 2004 event. In addition to the difference in still water level (0.8 m at high tide, Figure 4), the wave peak direction exhibits a large difference (56°) with $D_p = 200^\circ$ and $D_p = 256^\circ$, at high tide, for the 2004 and 2008 events, respectively. However, we should keep in mind that this is for an offshore location, south of Groix Island (star in Figure 1a). When the waves propagate and approach the coast, they refract and exhibit a much smaller difference in terms of direction, with, for instance, a difference of 14° at point P (Figure 1b), after the WW3 model results. Arriving at the coast, the differences are even smaller, ranging from 2 to 6° , for instance, along the main beaches (Grande Plage and Goerem) at about 45 m from the shoreline. Thus, the large offshore wave direction difference may not induce large differences in the induced wave overtopping volume, in the present case where offshore waves come from the southwest quadrant. However, in future work, it may be interesting to investigate a wider variety of wave direction (for instance, with waves coming from the northwest quadrant) and wave spectra, including measured ones, to further quantify the effect of the wave stochasticity on the flood. Such work would require a significant amount of computational resources.

We should also notice that the site of Gâvres is characterized by a topographic depression, such that the depression is filling up with the water entering inland and a large increase in water volume results in a slight increase of flooded surface. On other sites, characterized, for instance, by a coastal dune and, behind a flat land, the effect of the stochastic character of waves on the flood extent would be much more visible because slight changes in water volumes would induce large changes in the flood extent.

In terms of forecast and early warning, the finding implies that the wave stochasticity can have a significant effect on the flood intensity and, as much as possible, should be taken into account for sites known to be mainly flooded by wave overtopping. To face computational time issues, a meta-modeling approach could be used [31]. For coastal adaptation to increased flood hazards due to sea-level rise,

this also highlights that for sites dominated by wave overtopping, the stochastic character of waves has an effect larger than the one of sea-level rise on near term timeframes, that is, as long as the sea-level rise induces a still water level below the thresholds for overflow. This implies that lower confidence should be attributed to flood projections done on sites where the still water level remains below (or close to) the thresholds for overflow. However, as soon as overflow becomes the main flooding regime, the effects of climate change and the need for adaptation will become obvious. In the present study, we showed that for the 2004 and 2008 events and a DEM representative of the 2008 site configuration, the effect of the wave stochasticity on the water volume entering inland at high tide on a short time scale of 15 min would become smaller (but not negligible) than the effect of the sea-level rise effect for a sea-level increase larger than 1 m and 0.2 m, respectively, i.e., given the current and projected rates of sea-level rise [24], corresponding to sea-level rise that could be reached at the end of the century and around the mid-century, respectively. This conclusion holds for the 2008 coastal defense system. However, the coastal defense system height at Gâvres has been increased by at least 0.6 m since 2009, and adaptation will continue in the future, suggesting that, for the 2004 and 2008 reference events, the dominance of the effect of the wave stochasticity will last even longer.

As a conclusion, on the study site of Gâvres, we clearly show that the effect of the stochastic character of waves on the flood itself is far to be negligible and, especially on short time scale (~ 15 min), is comparable to the one of the sea-level rise as long as the still water level remains smaller than the critical level above which overflow occurs.

Supplementary Materials: The following are available online at <http://www.mdpi.com/2077-1312/8/10/798/s1>. Figure S1: An animation of the simulated flood for the 2008 event.

Author Contributions: Conceptualization, D.I.; formal analysis, D.I.; funding acquisition, D.I.; investigation, D.I.; methodology, D.I., J.R. and G.L.C.; project administration, D.I.; software, D.I. and R.P.; validation, D.I. and R.P.; visualization, D.I.; writing—original draft, D.I.; writing—review and editing, R.P., J.R. and G.L.C. All authors have read and agreed to the published version of the manuscript.

Funding: This research was funded by Agence National de la Recherche (ANR) grant ANR-16-CE04-0011 (RISCOPE project) and by BRGM.

Acknowledgments: The following data providers are acknowledged: LEGOS, NOAA, LOPS-IFREMER, SHOM. The authors are also grateful to Sylvestre Le Roy for his contribution to the SWASH implementation and some of the coastal defense photos.

Conflicts of Interest: The authors declare no conflict of interest. The funders had no role in the design of the study; in the collection, analyses, or interpretation of data; in the writing of the manuscript, or in the decision to publish the results.

References

1. Le Roy, S.; Pedreros, R.; André, C.; Paris, F.; Lecacheux, S.; Marche, F.; Vinchon, C. Coastal flooding of urban areas by overtopping: Dynamic modelling application to the Johanna storm (2008) in Gâvres (France). *Nat. Hazards Earth Syst. Sci.* **2015**, *15*, 2497–2510. [[CrossRef](#)]
2. Idier, D.; Rohmer, J.; Pedreros, R.; Le Roy, S.; Lambert, J.; Louisor, J.; Le Cozannet, G.; Le Cornec, E. Coastal flood: A composite method for past events characterisation providing insights in past, present and future hazards—joining historical, statistical and modelling approaches. *Nat. Hazards* **2020**, *101*, 465–501. [[CrossRef](#)]
3. Brown, J.D.; Spencer, T.; Moeller, I. Modeling storm surge flooding of an urban area with particular reference to modeling uncertainties: A case study of Canvey Island, United Kingdom. *Water Resour. Res.* **2007**, *43*, W06402. [[CrossRef](#)]
4. Van der Meer, J.W.; Allsop, N.W.H.; Bruce, T.; De Rouck, J.; Kortenhaus, A.; Pullen, T.; Schüttrumpf, H.; Troch, P.; Zanuttigh, B. Manual on wave overtopping of sea defences and related structures. An overtopping manual largely based on European research, but for worldwide application. EurOtop, 2018. Available online: www.overtopping-manual.com (accessed on 12 October 2020).
5. Gallien, T.W.; Sanders, B.F.; Flick, R.E. Urban coastal flood prediction: Integrating wave overtopping, flood defenses and drainage. *Coast Eng.* **2014**, *91*, 18–28. [[CrossRef](#)]

6. Zijlema, M.; Stelling, G.; Smit, P. SWASH: An operational public domain code for simulating wave fields and rapidly varied flows in coastal waters. *Coast Eng.* **2011**, *58*, 992–1012. [\[CrossRef\]](#)
7. Grilli, A.R.; Westcott, G.; Grilli, S.T.; Spaulding, M.L.; Shi, F.; Kirby, J.T. Assessing coastal hazard from extreme storms with a phase resolving wave model: Case study of Narragansett, RI, USA. *Coast Eng.* **2020**, *160*, 103735. [\[CrossRef\]](#)
8. Tuah, H.; Hudspeth, R.T. Comparisons of numerical random sea simulations. *J. Waterw. Port Coast Ocean Div.* **1982**, *108*, 569–584.
9. McCabe, M.V.; Stansby, P.K.; Apsley, D.D. Random wave runup and overtopping a steep sea wall: Shallow-water and Boussinesq modelling with generalised breaking and wall impact algorithms validated against laboratory and field measurements. *Coast Eng.* **2013**, *74*, 33–49. [\[CrossRef\]](#)
10. Dodet, G.; Melet, A.; Ardhuin, F.; Bertin, X.; Idier, D.; Almar, R. The Contribution of Wind Generated Waves to Coastal Sea Level Changes. *Surv. Geophys.* **2019**, *40*, 1563–1601. [\[CrossRef\]](#)
11. Pearson, J.; Bruce, T.; Allsop, N. Prediction of wave overtopping at steep seawalls—Variabilities and uncertainties. *Proc. Waves* **2001**, *1*, 1797–1808.
12. Pullen, T.; Allsop, N.; Bruce, T.; Kortenhaus, A.; Schüttrumpf, H.; Van der Meer, J. *Eurotop Wave Overtopping of Sea Defences and Related Structures: Assessment Manual*; Environ Agency: London, UK, 2007.
13. Romano, A.; Bellotti, G.; Briganti, R.; Franco, L. Uncertainties in the physical modelling of the wave overtopping over a rubble mound breakwater: The role of the seeding number and of the test duration. *Coast Eng.* **2015**, *103*, 15–21. [\[CrossRef\]](#)
14. Williams, H.E.; Briganti, R.; Pullen, T. The role of offshore boundary conditions in the uncertainty of numerical prediction of wave overtopping using non-linear shallow water equations. *Coast Eng.* **2014**, *89*, 30–44. [\[CrossRef\]](#)
15. Thompson, D.A.; Karunarathna, H.; Reeve, D.E. Modelling Extreme Wave Overtopping at Aberystwyth Promenade. *Water* **2017**, *9*, 663. [\[CrossRef\]](#)
16. Cariolet, J.M. Inondation des Côtes Basses et Rives Associées en Bretagne: Vers une Redéfinition des Processus Hydrodynamiques liés aux Conditions Météo-Océaniques et des Paramètres Morphosédimentaires. Océan, Atmosphère. Ph.D. Thesis, Université de Bretagne occidentale, Brest, France, 2011.
17. Le Cornec, A.; Schoorens, J. *Etude de l'aléa submersion marine sur le site de la Grande Plage de Gâvres*; Technical Report; GEOS-DHI: Morbihan, France, 2007.
18. SWASH Team. SWASH USER MANUAL, SWASH version 6.01, TU Delft. 2019. Available online: <http://www.tudelft.nl/swash> (accessed on 12 October 2020).
19. Ardhuin, F.; Rogers, W.E.; Babanin, A.V.; Filipot, J.; Magne, R.; Roland, A.; Van der Westhuysen, A.; Queffelec, P.; Lefevre, J.; Aouf, L.; et al. Semiempirical dissipation source functions for ocean waves. Part I: Definition, calibration, and validation. *J. Phys. Oceanogr.* **2010**, *40*, 917–941. [\[CrossRef\]](#)
20. Lazure, P.; Dumas, F. An external-internal mode coupling for a 3D hydrodynamical model for applications at regional scale (MARS). *Adv. Water Resour.* **2008**, *31*, 233–250. [\[CrossRef\]](#)
21. Boudière, E.; Maisondieu, C.; Ardhuin, F.; Accensi, M.; Pineau-Guillou, L.; Lepesqueur, J. A suitable metocean hindcast database for the design of Marine energy converters. *Int. J. Mar. Energy* **2013**, *3–4*, e40–e52. [\[CrossRef\]](#)
22. Dee, D.P.; Balsameda, M.; Balsamo, G.; Engelen, R.; Simmons, A.J.; Thépaut, J.-N. Toward a consistent reanalysis of the climate system. *Bull. Am. Meteor. Soc.* **2014**, *95*, 1235–1248. [\[CrossRef\]](#)
23. Wilks, S.S. Determination of Sample Sizes for Setting Tolerance Limits. *Ann. Math. Stat.* **1941**, *12*, 91–96. [\[CrossRef\]](#)
24. Oppenheimer, M.B.; Glavovic, B.; Hinkel, J.; van de Wal, R.; Magnan, A.K.; Abd-Elgawad, A.; Cai, R.; Cifuentes-Jara, M.; DeConto, R.M.; Ghosh, T.; et al. Sea Level Rise and Implications for Low-Lying Islands, Coasts and Communities. In *IPCC Special Report on the Ocean and Cryosphere in a Changing Climate*; Pörtner, H.-O., Roberts, D.C., Masson-Delmotte, V., Zhai, P., Tignor, M., Poloczanska, E., Mintenbeck, K., Alegria, A., Nicolai, M., Okem, A., et al., Eds.; IPCC—Intergovernmental Panel on Climate Change: Geneva, Switzerland, 2019.
25. De Conto, R.M.; Pollard, D. Contribution of Antarctica to past and future sea-level rise. *Nature* **2016**, *531*, 591–597. [\[CrossRef\]](#)

26. Stammer, D.; Van de Wal, R.S.W.; Nicholls, R.J.; Church, J.A.; Le Cozannet, G.; Lowe, J.A.; Horton, B.P.; White, K.; Behar, D.; Hinkel, J. Framework for high-end estimates of sea level rise for stakeholder applications. *Earths Future* **2019**, *7*, 923–938. [[CrossRef](#)]
27. Jevrejeva, S.; Frederikse, T.; Kopp, R.E.; Le Cozannet, G.; Jackson, L.P.; van de Wal, R.S.W. Probabilistic sea level projections at the coast by 2100. *Surv. Geophys.* **2019**, *40*, 1673–1696. [[CrossRef](#)]
28. Bamber, J.L.; Oppenheimer, M.; Kopp, R.E.; Aspinall, W.P.; Cooke, R.M. Ice sheet contributions to future sea-level rise from structured expert judgment. *Proc. Natl. Acad. Sci. USA* **2019**, *116*, 11195–11200. [[CrossRef](#)] [[PubMed](#)]
29. Poulter, B.; Halpin, P.N. Raster modelling of coastal flooding from sea-level rise. *Int. J. Geogr. Inf. Sci.* **2008**, *22*, 167–182. [[CrossRef](#)]
30. Didier, D.; Baudry, J.; Bernatchez, P.; Dumont, D.; Sadegh, M.; Bismuth, E.; Bandet, M.; Dugas, S.; Sévigny, C. Multihazard simulation for coastal flood mapping: Bathtub versus numerical modelling in an open estuary, Eastern Canada. *J. Flood Risk Manag.* **2019**, *12*, e12505. [[CrossRef](#)]
31. Rohmer, J.; Idier, D.; Pedreros, R. A nuanced quantile random forest approach for fast prediction of a stochastic marine flooding simulator applied to a macrotidal coastal site. *Stoch. Environ. Res. Risk Assess.* **2020**, *34*, 867–890. [[CrossRef](#)]

Publisher's Note: MDPI stays neutral with regard to jurisdictional claims in published maps and institutional affiliations.



© 2020 by the authors. Licensee MDPI, Basel, Switzerland. This article is an open access article distributed under the terms and conditions of the Creative Commons Attribution (CC BY) license (<http://creativecommons.org/licenses/by/4.0/>).